Tuning the electronic properties of $LaAlO_3/SrTiO_3$ interfaces by irradiating the $LaAlO_3$ surface with low-energy cluster ion beams

Karl Ridier,[1,2,*] Damien Aureau,[2] Bruno Bérini,[1] Yves Dumont,[1] Niels Keller,[1] Jackie Vigneron,[2] Arnaud Etcheberry,[2] Bernadette Domengès,[3] and Arnaud Fouchet[1,†]

[1]*Groupe d'Étude de la Matière Condensée (UMR 8635), Université de Versailles Saint-Quentin-en-Yvelines–CNRS–Université Paris-Saclay, 45 Av. des États-Unis 78035 Versailles, France*

[2]*Institut Lavoisier de Versailles (UMR 8180), Université de Versailles Saint-Quentin-en-Yvelines–CNRS–Université Paris-Saclay, 45 Av. des États-Unis 78035 Versailles, France*

[3]*LAMIPS - CRISMAT - NXP Semiconductors - Presto-Engineering Europe Joint Laboratory, CNRS-UMR6508, ENSICAEN, UCN, Presto-Engineering Europe, 2 rue de la Girafe, 14000 Caen, France*

(Received 23 May 2017; revised manuscript received 17 November 2017; published 19 January 2018)

We have investigated the effects of low-energy ion beam irradiations using argon clusters on the chemical and electronic properties of $LaAlO_3/SrTiO_3$ (LAO/STO) heterointerfaces by combining x-ray photoelectron spectroscopy (XPS) and electrical transport measurements. Due to its unique features, we demonstrate that a short-time cluster ion irradiation of the LAO surface induces significant modifications in the chemical properties of the buried STO substrate with (1) a lowering of Ti atoms oxidation states (from Ti^{4+} to Ti^{3+} and Ti^{2+}) correlated to the formation of oxygen vacancies at the LAO surface and (2) the creation of new surface states for Sr atoms. Contrary to what is generally observed by using higher energy ion beam techniques, this leads to an increase of the electrical conductivity at the LAO/STO interface. Our XPS data clearly reveal the existence of dynamical processes on the titanium and strontium atoms, which compete with the effect of the cluster ion beam irradiation. These relaxation effects are in part attributed to the diffusion of the ion-induced oxygen vacancies in the entire heterostructure since an increase of the interfacial metallicity is also evidenced far from the irradiated area. This paper highlights the possibility of tuning the electrical properties of LAO/STO interfaces by surface engineering, confirming experimentally the intimate connection between LAO chemistry and electronic properties of LAO/STO interfaces.

DOI: 10.1103/PhysRevB.97.035146

I. INTRODUCTION

The quasi-2-dimensional electron gas (q-2-DEG) formed at the interface between the two band insulators $LaAlO_3$ (LAO) and $SrTiO_3$ (STO) [1] is one of the most fascinating systems in the field of oxide electronics. The LAO/STO heterostructure is the subject of intensive research due to its multifunctional properties, which open avenues for both fundamental and applied perspectives. Among its most interesting properties, the q-2-DEG is known to appear only when at least 3.5 unit cells (u.c.) of LAO are epitaxially deposited on TiO_2-terminated STO substrates [2]; this interface has shown to host ferromagnetism [3–6], two-dimensional superconductivity [7], and strong spin-orbit coupling [8,9]. Despite intense interest, many basic questions remain about the microscopic mechanisms that give rise to the q-2-DEG at the LAO/STO interface. Pure intrinsic electronic reconstruction due to polar discontinuity (known as the "polar catastrophe" model) [10], presence of oxygen vacancies in the STO substrate [11–13], or interfacial cation mixing [10,14,15] have been considered as possible mechanisms to, at least, partially explain the observed electronic properties of LAO/STO interfaces. Recently, an alternative model, based on first-principles calculations [16], suggests that the various experimental observations (including critical thickness, carrier density, interface magnetism) originate from an intricate balance between surface oxygen vacancies in LAO and cation antisite defects thermodynamically induced by the polar discontinuity across the interface.

While these mechanisms and their relative importance are still under debate, the LAO/STO heterostructure is particularly promising for applications because of the intrinsic confinement of the electronic properties at the interface and the possibility to control the electrical conductivity at the local scale. For instance, a tunable metal-insulator ground state has been evidenced in LAO/STO by using the electric field effect [2,17,18]. Moreover, several observations reveal that the LAO surface (surface states and defects) strongly influences the properties of the interfacial q-2-DEG. As an example, the electronic properties of LAO/STO interfaces have been tailored by conducting atomic force microscopy (AFM) [19,20], by deposition of surface adsorbates on the LAO film [21,22], by protonation of the LAO surface [23], or by creation of

*Corresponding author: karl.ridier@hotmail.fr; Present address: Laboratoire de Chimie de Coordination, CNRS UPR–8241, 205 route de Narbonne, F–31077 Toulouse, France.

†Corresponding author: arnaud.fouchet@ensicaen.fr; Present address: Laboratoire de Cristallographie et Sciences des Matériaux (UMR 6508), Normandie Université, ENSICAEN (Ecole Nationale Supérieure d'Ingénieurs de Caen), UNICAEN (Université de Caen), CNRS, 6 Bd. Maréchal Juin, F–14050 Caen, France.

surface defects, as predicted by density functional theory (DFT) calculations of LAO/STO heterostructure [16] and other interfaces such as $NdAlO_3/SrTiO_3$ [24]. This is an intriguing feature that a surface modification can remotely influence the interfacial electronic properties. A better understanding of this general effect is crucial: (1) as a fundamental point of view to bring new insights in the origin of the q-2-DEG and its properties and (2) for applications as sensor or electronic devices, since small surface modifications or defects can lead to a sizeable change in the interfacial electronic properties.

Ion beam irradiation is a promising way to modify the surface properties of materials. In recent years, ion beam exposure has emerged as a novel tool to tailor the structural, mechanical, electronic, and even magnetic properties of materials by inducing atomic defects in a controlled manner. In particular, ion irradiation of oxide materials has been used for both device fabrication and material modification [25,26]. In LAO/STO, ion beam irradiation processes have been essentially used to induce metal-to-insulator transitions at the interface by creating defects (amorphization, local disorder) and strains in the heterostructure, either by using 150–350 eV monoatomic argon ions [27,28], low-Z (2-MeV hydrogen and 500-keV helium) ions [29], or 50-keV oxygen ions [30] (see Table SI-1 in part 1 of the Supplemental Material [31]). These techniques have been advantageously used for nano-patterning channels in which the original properties of the q-2-DEG (electrical conductivity, superconductivity) were preserved, opening interesting prospects for the realization of mesoscopic devices. In these previous studies, the metal-insulator transition was described as the consequence of the large penetration lengths and experienced ion implantation, which cause strong charge carrier localizations via ion-induced defects and structural changes in the heterostructure.

In this paper, we explore the appealing features of *argon cluster ion beams* (annotated Ar_n^+, with $n = 1000-2000$ at./cluster) to irradiate the upper surface of LAO/STO heterostructures. Compared to monoatomic ion beam sputtering techniques, the main feature is that the average energy per argon atom is considerably low (only few eV per atom), leading to small penetration lengths into the sputtered material. The cluster ion beam sputtering technique has already been used on organic and polymer materials [32,33] and as a promising tool to prepare oxide surfaces [34] or to perform depth profiling with low amount of defects in perovskite oxides such as $SrTiO_3$ [35]. In particular, this sputtering process has proved to strongly limit ion implantation in oxide materials.

We have combined x-ray photoelectron spectroscopy (XPS) and electrical measurements to investigate the effects of cluster-ion-beam-induced modifications on both the chemical and physical (electrical) properties of LAO/STO heterointerfaces. Due to its unique features, we demonstrate that this low-energy sputtering technique can be advantageously used to tune the chemical and electronic properties of LAO/STO interfaces. Due to the effective attenuation length (EAL) L of the photoemitted electrons ($L \approx 2.05$ nm in LAO and STO at the used photon energy) [36], XPS gives valuable information about the physicochemical properties of the buried interface through the LAO film. We have studied three 4.7-nm-thick ($\sim$12−13 u.c.) heterostructures (hereafter denoted H1, H2, and H3), grown under slightly different conditions to provide interfaces with different initial electrical properties (see Sec. II, for details). This thickness was chosen as a good compromise to be able to have thick enough LAO film to preserve the interface from direct ion beam irradiation while still being thin enough to probe the entire heterostructure by XPS.

In the first part of this paper (Sec. III), the XPS depth-profiling analysis of a LAO/STO heterostructure by the Ar cluster ion beam sputtering technique is performed up to the complete etching of the LAO film. These first results give some insights on the evolution of the chemical and physical properties of the LAO/STO system during the cluster ion exposure. In the second part (Sec. IV), we have investigated the effects of a short-time cluster ion irradiation on the electronic behavior of LAO/STO interfaces, and the possibility to tune the electrical properties of the q-2-DEG is addressed. Importantly, the crucial role played by ion-induced oxygen vacancies as well as the existence of dynamical (relaxation) processes are demonstrated.

II. EXPERIMENTAL METHODS

A. Sample preparation

The $LaAlO_3/SrTiO_3$ (001) samples were prepared by pulsed laser deposition (PLD) by ablating a single crystal LAO target onto TiO_2-terminated STO (001) substrates. The laser (KrF excimer laser, $\lambda = 248$ nm) energy density was set to $1.8\,J/cm^2$ with a repetition rate of 1 Hz. The substrates were heated to 740 °C, and the oxygen partial pressure was set to 1.33×10^{-5} mbar during deposition. Three 4.7-nm-thick ($\sim$12−13 u.c.) heterostructures (denoted H1, H2, and H3) have been grown. Immediately after deposition, heterostructures H1 and H2 were annealed for 1 h at 540 °C and 0.2 mbar of pure oxygen, whereas sample H3 was not annealed. The preparation of the TiO_2-terminated STO substrates comprised the following steps: (1) a first annealing at 950 °C for 1 h with an oxygen flow; (2) an immersion of the substrates in demineralized water for 10 min, followed by a short (30 s) dip in a buffered NH_4F-HF solution; and (3) a final annealing under the same conditions.

B. The XPS measurements and cluster ion beam irradiation

The XPS measurements were carried out using an ESCALAB 250 Xi spectrometer with a monochromatic Al-Kα x-ray source ($h\nu = 1486.6$ eV). The photoelectron EALs are very close in STO and LAO at this photon energy and can be taken equal to $L_{LAO} \approx L_{STO} \approx 2.05$ nm [36]. The detection was performed perpendicularly to the sample surface using a constant energy analyzer mode (pass energy 20 eV), and spectra were recorded with a 0.1 eV energy step size. Because of unavoidable charging effects, in particular for insulating samples, a low-energy electron flood gun was used for all samples to perform experiments in the same conditions. Because of resulting uncertainties in the absolute binding energies, all XPS spectra have been aligned, considering the main O 1*s* core-line as the reference at 530.7 eV, as reported in the literature.

Argon cluster ion beam irradiations were performed using the MAGCIS Dual Beam ion source. The average kinetic energy of each cluster (two sizes were used: $\sim$1000 and

~2000 atoms per cluster) was fixed to 8000 eV. The incoming argon clusters reached the sample with an angle of 30° from the surface normal, and the ion current density was fixed to ~15 μA/cm^2. The LAO/STO heterostructures were irradiated on a square area of ~3.25 × 3.25 mm^2, while the size of the XPS analysis zone was 650 × 650 μm^2 in the center of this irradiated area. Quantification was performed based on the O 1s, C 1s, Ar 2p, Sr 3d, Ti 2$p_{3/2}$, La 4d, and Al 2p peak areas after a Shirley type background subtraction using the Thermo Fisher Scientific Avantage© data system.

C. Electrical characterization

Sheet resistance measurements were carried out in a four-point configuration in the temperature range 2–300 K using a Quantum Design PPMS system. The interfaces were contacted by ultrasonic bonding with Al wire. The Al wire penetrates into the sample from the top surface and makes connection across the interface that enables us to probe the LAO/STO interfacial conductivity. Hall effect measurements were performed using the Van der Pauw method to extract the carrier density by applying a ±9T magnetic field perpendicular to the interface plane. The resistivity data was antisymmetrized according to the applied magnetic field in order to exclude the longitudinal ρ_{xx} component.

D. Atomic force microscopy (AFM)

Topography and roughness of the samples have been investigated by AFM (Brucker Dimension 3100) in tapping mode using commercial tips with 300 kHz resonant frequency and 40 N/m spring constant.

E. Transmission electron microscopy–scanning transmission electron microscopy (TEM-STEM)

Thin lamella was prepared in a Dual-Beam system (FEI-HELIOS 600, Elstar Field Emission Scanning Electron Microscope column and Tomahawk focused Ga ion beam column) equipped with an Easy-lift manipulator designed for *in-situ* lift-out thin lamella preparations and an energy dispersive x-ray spectroscopy (EDS) elemental analysis system (OXFORD–AZTEC). This preparation technique allows one to keep the integrity of most parts of the sample. The TEM-STEM study was performed on a JEM-ARM200F microscope, operating at 200 kV, equipped with a cold FEG and double TEM-STEM Cs correctors (ensuring a lattice TEM or STEM image resolution below 0.1 nm), and a JEOL EDS system (for concentration line profiles, the electron nano-beam diameter was below 0.15 nm at the entrance surface of the lamella).

III. XPS DEPTH-PROFILING ANALYSIS OF A LAO/STO HETEROSTRUCTURE: EFFECTS OF THE CLUSTER ION EXPOSURE ON THE CHEMICAL PROPERTIES

In this first part of this paper, we have studied the effects of the argon cluster ion sputtering technique in the XPS depth-profiling analysis of the heterostructure H1 (see details in Sec. II). In this preliminary experiment, a complete etching of the LAO film has been performed. The use of Ar clusters (~1000 at./cluster) with a mean energy of 8000 eV (i.e., ~8 eV per incoming Ar atom) is necessary to completely etch the LAO layer in a reasonable time. The total counting time to obtain all XPS spectra with a satisfying signal-to-noise ratio between each etching step is about 12 min.

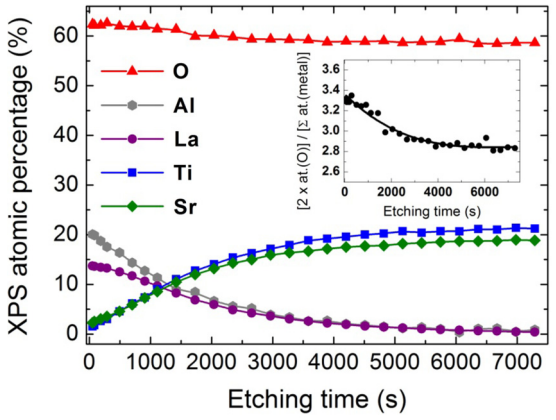

FIG. 1. Time evolution of the XPS atomic percentage of the different detected elements along the argon cluster ion depth profiling of the heterostructure H1. Inset: time evolution of the ratio [2 × %at(O)]/[%at (Sr) + %at (Ti) + %at (La) + %at (Al)]. The solid line is a guide for the eye.

A. General results

Figure 1 shows the time evolution of atomic percentages measured by XPS along the cluster ion beam irradiation. The progressive and complete disappearance of the La and Al elements is evidenced, while, in the same time, the XPS signal of Sr and Ti atoms is enhanced. As already reported [34,35], no signal of argon is detected by XPS during the depth profiling, showing that the cluster ion exposure does not generate measurable implantation into the heterostructure in the XPS detection limit (% at (Ar) < 0.1%).

The time evolution of the LAO film thickness can be estimated along the depth profile from the XPS atomic percentage of metal cations and the photoelectron EALs in LAO and STO (see part 2.1 of the Supplemental Material [31]). Although these calculations are approximate, we can estimate that the complete etching of the LAO film is reached after an irradiation of ~3000 s (i.e., with a sputter rate of about 0.95 Å/min in LAO). After 3000 s, a residual amount of La and Al is still detected, likely because the interface is not perfectly abrupt and is possibly destructured by the ion sputtering. Interestingly, a significant decrease of the atomic percentage of oxygen is observed from 62.2% to 58.6% throughout the depth profiling. This effect is better highlighted in the inset of Fig. 1, which displays the evolution of the ratio [2 × %at(O)]/[%at (Sr) + %at (Ti) + %at (La) + %at (Al)] as a function of irradiation time. Although the sample H1 was annealed in oxygen after deposition, this ratio decreases by 15%, indicating the formation of a sizeable amount of oxygen vacancies in the heterostructure due to the cluster ion exposure.

The XPS spectra of the La 4d and Al 2p core-line peaks are presented in the Supplemental Material (Fig. SI-1 [31]) at different times of the ion beam irradiation of H1. These data show the progressive decrease and the total vanishing of the La and Al peaks with sputtering time, but no noticeable evolution

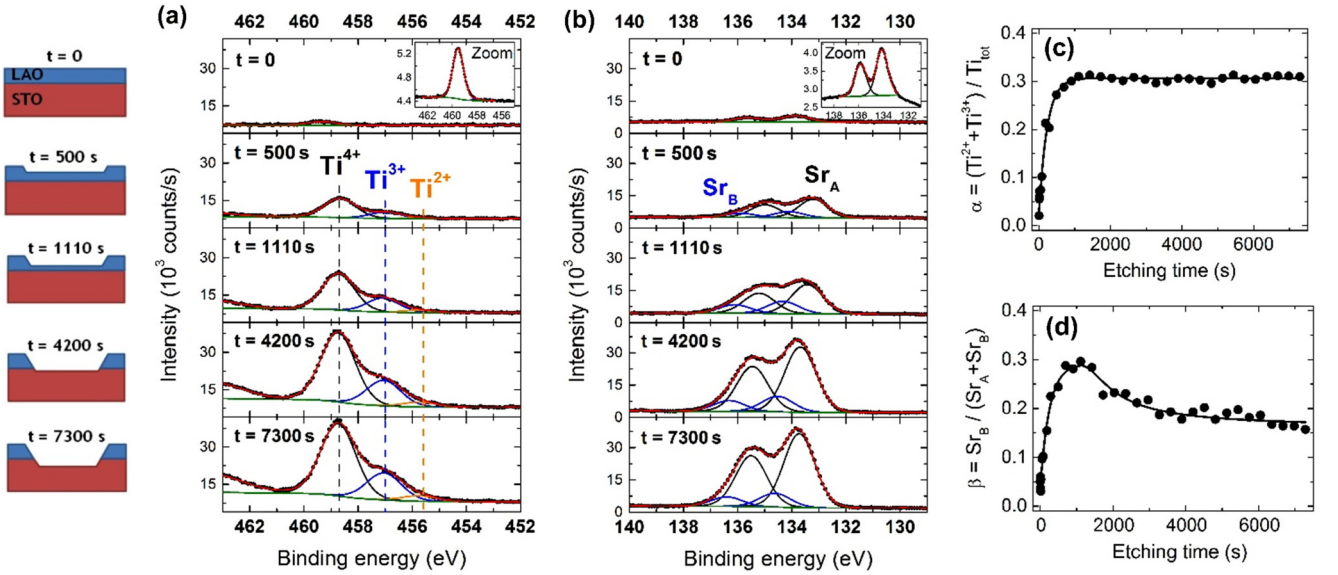

FIG. 2. Influence of the cluster ion beam exposure on titanium and strontium atoms during the complete depth profiling of the heterostructure H1. (a) and (b) The XPS spectra of the Ti $2p_{3/2}$ and Sr $3d$ peaks, respectively, at different etching times. The sketches on the left schematically represent the depth of the ion etching at each step. The insets (at $t = 0$) show high-resolution (pass energy 10 eV) measurements of Ti $2p_{3/2}$ and Sr $3d$ spectra (with a counting time of ~2 h) performed prior to the beginning of the ion sputtering. The total counting time between each etching step was then fixed to 12 min. (c) and (d) Evolution of the $\alpha = [Ti^{3+} + Ti^{2+}]/[Ti^{4+} + Ti^{3+} + Ti^{2+}]$ and $\beta = Sr_B/[Sr_A + Sr_B]$ ratios, respectively, as a function of etching time (solid lines are guides for the eye).

is detected on the peak shape throughout the depth profiling. By comparison, as shown in Fig. 2, strong modifications are evidenced on the XPS Ti $2p_{3/2}$ and Sr $3d$ core-lines. These spectra are displayed in Figs. 2(a) and 2(b), respectively, at different etching times. The total peak intensities progressively increase with time, in the early stages of the irradiation, as the upper LAO film is progressively etched by the ion bombardment.

B. Titanium

As displayed in Fig. 2(a), the Ti $2p_{3/2}$ peak at $t = 0$ mainly consists of a Ti^{4+} line, while a very small component (<2%) of Ti^{3+} can be eventually extracted from XPS data. As soon as the beginning of the cluster ion etching, we clearly observe the appearance of two low-binding energy components (at $\Delta E = 1.7 \pm 0.1$ eV and 3.0 ± 0.1 eV) associated to lower oxidation states (Ti^{3+} and Ti^{2+}, respectively) of titanium atoms. Continuous lines in Fig. 2(a) are the best fits assuming the same full width at half maximum (FWHM) for the Ti^{4+}, Ti^{3+}, and Ti^{2+} peaks. From the analysis of the fits, the time evolution of the ratio of the peak areas $\alpha = [Ti^{3+} + Ti^{2+}]/[Ti^{4+} + Ti^{3+} + Ti^{2+}]$ is represented in Fig. 2(c). This ratio grows rapidly to reach 30% at $t \approx 1000$ s and then remains stable until the end of the depth profiling. The change in the XPS Ti $2p_{3/2}$ spectra can also be correlated to the modifications observed in the valence band spectra (see Fig. SI-2 of the Supplemental Material [31]). In particular, the growth of a band of defect states occurs in the band gap region due to the cluster ion exposure. This feature has already been observed resulting from ion irradiation in STO [35,37]. These in-gap states signal the presence of $3d$ charge carriers near the interface in STO associated with the Ti^{3+} and Ti^{2+} ions [38,39].

The lowering of oxidation states of titanium atoms is a well-known effect of ion beam exposures on STO substrates, especially using high-energetic monoatomic ions [34,35,40,41]. This effect is commonly attributed to the creation of oxygen vacancies in STO, which result in an insulator-to-metal transition and high-mobility surface conduction [42–44]. Indeed, each oxygen vacancy releases two electrons that can occupy the initially empty Ti $3d$ band states [37,45], resulting in Ti^{3+} or even Ti^{2+} low-binding energy components.

By way of comparison, we have carried out a similar ion beam irradiation, using 8000 eV argon clusters, on a bare STO substrate. This depth profile has been realized in the *same experimental conditions* as for the LAO/STO heterostructure H1: same cluster size (1000 at./cluster), energy (8000 eV/cluster), and incoming current density (~15 μA/cm^2). Although the comparison should not be considered as apples-to-apples since the bare STO substrate and the heterostructure H1 have been exposed to different external environments (vacuum, temperature), these comparative experiments, presented in part 2.3 of the Supplemental Material [31], provide interesting indications. As shown in Fig. SI-3 of the Supplemental Material [31], the cluster ion irradiation also induces lower oxidation states of Ti and thus generates oxygen vacancies into STO. Nevertheless, the ratio α reaches only 13.5% in the stationary regime, i.e., a lower value than that obtained for the LAO/STO interface (30%) (see discussion in the Supplemental Material [31]). In LAO/STO, the large value of the ratio α and the formation of a significant Ti^{2+} component signal the presence of a great amount of oxygen vacancies near the interface in the buried STO substrate. Interestingly, compared

to the STO substrate, the creation of oxygen vacancies in the heterostructure seems to be significantly amplified by the presence of the upper LAO film.

C. Strontium

A careful investigation of the XPS Sr 3*d* core-line has also been conducted. As shown in Fig. 2(b), at $t = 0$ (see the inset), we can conveniently describe the Sr 3*d* peak by a unique doublet arising from the spin-orbit coupling. The energy difference between the Sr $3d_{5/2}$ and Sr $3d_{3/2}$ components is around 1.76 eV, and their intensity ratio is, as expected, equal to ca. 1.5. In the same way as for the Ti $2p_{3/2}$ peak, the Sr 3*d* core-line is rapidly and strongly modified under the effect of the cluster ion beam exposure. The XPS data clearly show the emergence of an additional high-binding energy doublet (hereafter denoted Sr_B), which progressively grows during the cluster ion sputtering. This Sr_B component signals the appearance of a new chemical environment for the Sr atoms. Continuous lines in Fig. 2(b) show the results of the best fits considering two doublets for the Sr 3*d* core-line. Fits were realized imposing the same FWHM for all components and an energy shift equal to 0.85 ± 0.05 eV between the two doublets [40,41,46,47]. The time evolution of the ratio of the doublet areas $\beta = Sr_B/[Sr_A + Sr_B]$ is presented in Fig. 2(d). This ratio increases up to 28% after ∼700 s of etching, reaches a small plateau between 700 s and 1500 s, and finally decreases slowly to ∼18% .

Such a modification (growth of a high-binding energy doublet) of the Sr 3*d* core-line due to the ion beam irradiation has already been evidenced on STO substrates [34,40,41]. In STO, this Sr_B doublet is associated with the existence of a surface component of Sr atoms, which tend to migrate toward the outermost surface as a result of the energy supplied by the incoming Ar ions [34,46–48]. Interestingly, *the same effect occurs in LAO/STO* even though the STO substrate is covered by the LAO film. This has been evidenced by complementary low-energy He^+ ion scattering (LEIS) experiments. This technique is unique in its sensitivity to both structure and elemental composition of extreme surfaces and gives precise information on the chemical nature of the first atomic layer encountered by the helium ions projectiles. Figure 3 shows the LEIS spectra recorded on a pure STO substrate (black curve) and on LAO/STO at different etching times, during the first stages of the cluster ion exposure ($t < 600$ s, while the LAO film is not totally etched).

The spectrum obtained on the pure STO substrate exhibits two main peaks around 680 and 800 eV, corresponding to titanium and strontium atoms, respectively [49]. As for the LAO/STO heterostructure, the spectrum at $t = 0$ shows the existence of two peaks around 530 and 860 eV associated to aluminum and lanthanum atoms. Upon cluster ion exposure, a slight decrease of the Al intensity is evidenced as well as a gradual increase of the intensity around 800 eV, which is attributed to the presence of Sr atoms at the outermost LAO surface. No visible changes are observed in the Ti and La regions. These results strongly support the fact that the cluster ion exposure causes the migration of strontium atoms toward the outermost surface (through the LAO film), confirming the changes observed in the XPS Sr 3*d* spectra. Furthermore, by comparing the XPS results obtained (in the same experimental conditions) on a bare STO substrate (see Fig. SI-4 of the Supplemental Material [31]), we can argue that the singular evolution of the ratio β [shown in Fig. 2(d)] is also compatible with the formation of a Sr component at the LAO surface (see the discussion in part 2.3 of the Supplemental Material [31]).

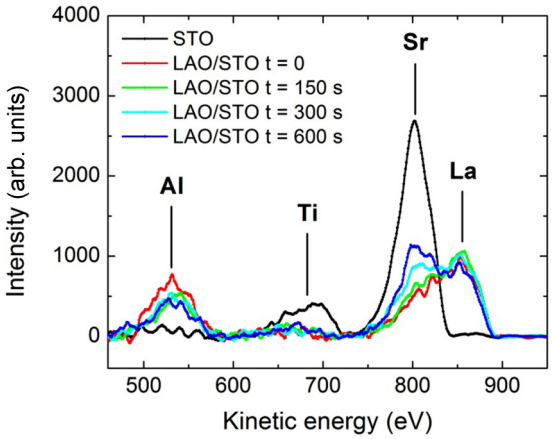

FIG. 3. The LEIS spectra (978-eV He^+ ions, scattering angle of 130°) recorded on the STO surface (black curve) and a LAO/STO heterostructure at different times of the cluster ion beam exposure (2000 at./cluster, mean energy 4000 eV/cluster). Data have been normalized and corrected from the background.

D. Discussion

In this first part, we have investigated by XPS and LEIS the effects of an argon cluster ion beam exposure on the heterostructure H1 during the complete depth profiling of the LAO film. This low-energy sputtering technique presents unique features (very low sputter rates and no argon implantation) and is known to act merely on the outermost surface of oxide materials, inducing progressive etching with relatively low defect levels [34,35]. Despite these particular characteristics, strong modifications occur on the Ti and Sr atoms, as revealed by XPS data, while, interestingly, no visible changes in the chemical environment of aluminum and lanthanum are detected during the ion exposure.

The most striking observation is that these modifications on Ti and Sr mainly occur in the first 700–900 s of etching, while the LAO film is not totally etched. At $t = 900$ s, the LAO thickness is, for instance, estimated to be ∼3.0 nm. Therefore, it seems that chemical modifications on Ti and Sr atoms occur even though the STO substrate *does not undergo directly* the effects of the incoming clusters. These observations strongly suggest that the argon clusters cause defects in the LAO layer (while physical etching occurs), which in turn generate modifications in the buried STO.

For titanium, the lowering of the mean oxidation state is clearly related to the formation of oxygen vacancies into the LAO/STO heterostructure. This is corroborated by the observation of a noticeable decrease of the oxygen content in the heterostructure during the etching process (see Fig. 1). Moreover, as demonstrated by the comparative experiment performed on a bare STO substrate in the same irradiation conditions, these effects seem to be amplified by the presence

of the upper LAO layer, presumably because the activation energy to create oxygen vacancies is lower in the LAO film deposited on STO than in the bare STO substrate. The most likely explanation is that a great amount of oxygen vacancies is created in the LAO layer by the cluster ion exposure, generating a large concentration gradient. These oxygen vacancies are then transferred by diffusion into the STO, leading to a lowering of the oxidation states of buried Ti atoms. These diffusion phenomena will be more thoroughly evidenced and discussed in the second part of this paper. As for strontium, XPS and LEIS data show the progressive migration of Sr atoms toward the outermost surface through the LAO film. The mechanism responsible for this effect is not completely understood. We can speculate that it may be related to a diffusion process, possibly stimulated by the selective sputtering of Al atoms in the LAO film by the cluster ion irradiation (*vide infra*).

These first observations support recent studies [16], which predict that LAO/STO heterostructures are stabilized by the intricate balance of surface and interface defects. In the present case, the low-energy cluster ion beam irradiation induces significant modifications in the LAO layer, which tend to destabilize the thermodynamic equilibrium of the heterostructure. Our XPS data show that the chemical properties of the interface (on the STO side) are then strongly affected to compensate the imbalance produced by the ion exposure. At this point, it appears intriguing to investigate the evolution of the electronic properties at the interface, in particular during the first steps of the ion-beam exposure when the chemical properties of STO are modified below the LAO film. This analysis is the purpose of the next part of this paper.

IV. SHORT-TIME ARGON CLUSTER ION EXPOSURE ON LAO/STO: MONITORING OF THE INTERFACIAL CONDUCTIVITY

In this second part, we have investigated the evolution of the electronic properties of LAO/STO interfaces under the effect of a *short-time* argon cluster ion beam exposure. For that particular purpose, two 4.7-nm-thick LAO/STO samples (hereafter denoted H2 and H3) have been studied. Both interfaces were grown under identical conditions except that H2 was annealed for 1 h at $T = 540\,^{\circ}\mathrm{C}$ and $P(O_2) = 0.2$ mbar of pure oxygen immediately after deposition, whereas H3 was not annealed (see Sec. II, for details). As a result, the two interfaces exhibit different initial electrical properties. For both samples, the LAO film was deposited on two distinct areas over the $10 \times 4\ \mathrm{mm}^2$ STO substrate, separated from each other by a 2-mm bare STO region. A schematic representation of H2 and H3 samples is given in Fig. 4(a). After deposition, AFM images confirmed the smoothness of the as-deposited surfaces and the presence of well-defined single-u.c. high step terraces for both samples [see Figs. SI-5(a) and SI-6(a) in the Supplemental Material [31]].

The electrical transport properties of H2 and H3 are presented in Figs. 4(b) and 4(c). The temperature dependence of the sheet resistance is displayed in Fig. SI-10 in the Supplemental Material [31]. Initially, as shown in Fig. 4(b), the sheet resistance of the "annealed" sample H2 at room temperature ($R_S = 968\,\mathrm{k}\Omega/\square$) is found to be two orders of magnitude larger than that of the "not annealed" sample H3 ($R_S = 17.5\,\mathrm{k}\Omega/\square$). As displayed in Fig. SI-10 (black curves) of the Supplemental Material [31], H3 presents a

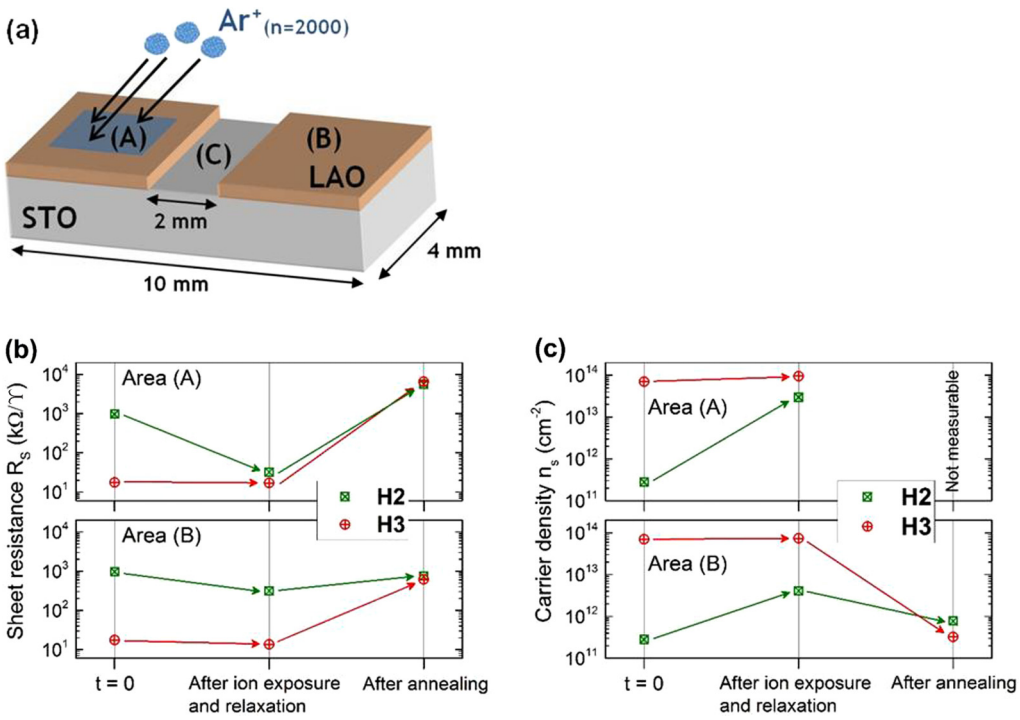

FIG. 4. (a) Schematic representation of the H2 and H3 samples. For each sample, zone (A) is defined as the ion-irradiated zone and (B) as the witness zone on the other side of the 2-mm bare STO area, denoted (C). (b) and (c) Evolution of the sheet resistance and carrier density, respectively, measured at room temperature on areas (A) (top panel) and (B) (bottom panel) of heterostructures H2 and H3 at different stages of the experiment ($t = 0$, after ion beam exposure and after annealing). Arrows help to indicate the evolution.

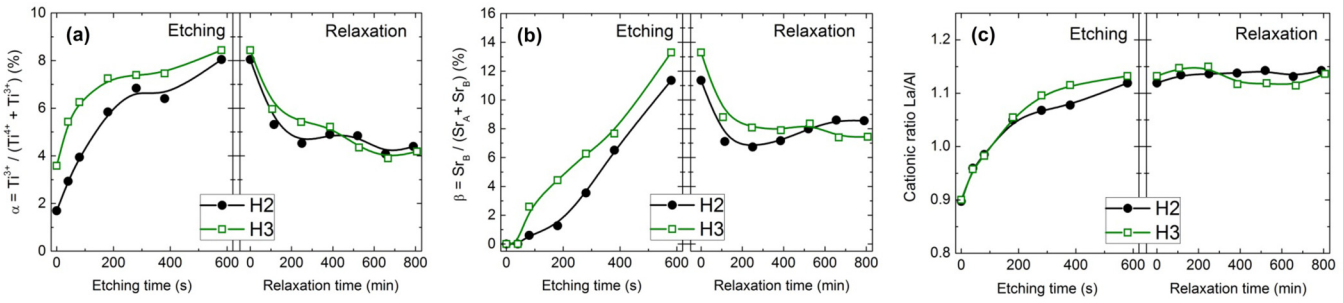

FIG. 5. The XPS results obtained on the irradiated area (A) of H2 and H3 during the cluster ion exposure and the following relaxation time. (a) and (b) Time evolution of the $\alpha = Ti^{3+}/[Ti^{4+} + Ti^{3+}]$ and $\beta = Sr_B/[Sr_A + Sr_B]$ ratios, respectively. (c) Evolution of the La/Al cationic ratio as a function of time. This ratio has been evaluated considering a stoichiometric single crystal of $LaAlO_3$ as a reference.

genuine metallic behavior characterized by an increase of the sheet resistance with temperature, whereas the annealed sample H2 shows an insulatinglike behavior. Carrier density measurements presented in Fig. 4(c) confirm the observed differences between H2 and H3. Before any irradiation, the sheet carrier density of H3 at room temperature ($n_s = 7.0 \times 10^{13}\,cm^{-2}$) is two orders of magnitude larger than that of H2 ($n_s = 2.8 \times 10^{11}\,cm^{-2}$). Moreover, for both samples, the two LAO/STO areas were found electrically disconnected, while the nondeposited area (C) remained insulating. Note also that the obtained interfaces are somewhat more resistive than those reported in the literature [50]. The reasons for such behavior have to be clarified. This effect might be due to the presence of residual SrO at the interface, possibly originating from the HF etching procedure of the STO substrates or the deposition conditions. It is also possible that the initial substrate quality was not optimal.

A. Cluster ion sputtering and relaxation processes

Ion sputtering was realized by using 8000 eV argon clusters with a size (∼2000 at./cluster) twice larger than the depth profiling of H1. The average energy per incoming argon atom was then ∼4 eV. The two samples were irradiated on a square area, denoted (A), of size $3.25 \times 3.25\,mm^2$ on one of the two deposited zones [see Fig. 4(a)]. Zone (B), located on the other side of the 2-mm bare STO area (C), can be defined as a witness area. For both samples, the etching time was set to 580 s. At the end of the ion exposure, the thickness of the LAO film on the irradiated area (A) was estimated by XPS to be ∼3.5 nm (∼9 u.c.), well above the critical thickness of 4 u.c., ensuring that eventual modifications in the electrical properties cannot be imputed to physical etching of the LAO film below this critical thickness. The XPS measurements were performed on the irradiated area (A) of H2 and H3 at different times of the ion beam exposure and during a waiting time of 800 min following the end of the ion sputtering. For this set of XPS measurements, the counting time between each etching step was increased to 68 min (instead of 12 min for H1) to improve the signal-to-noise ratio of the Ti $2p$ and Sr $3d$ spectra.

1. Evolution of the chemical/compositional properties

First, the question of argon implantation was investigated by XPS. As already mentioned for H1, a very tiny amount of implanted Ar is detected on the irradiated area (A) of both samples during the ion beam irradiation. Long counting times allow for the extraction of a fraction of argon <0.1% of the total percentage of detected species (see Fig. SI-7 of the Supplemental Material [31]), confirming that no significant implantation occurs during the irradiation process. Ti $2p_{3/2}$ and Sr $3d$ spectra are displayed in Figs. SI-8 and SI-9 of the Supplemental Material [31], for H2 and H3, respectively, at different stages of the experiment (at $t = 0$, at the end of the ion exposure, after the "relaxation" process, and after final annealing). As previously observed for H1, the ion sputtering induces a lowering of the mean oxidation state of Ti (from Ti^{4+} to Ti^{3+}) and a progressive growing of the surface component Sr_B for strontium. The time evolution of the ratios of the peak areas: $\alpha = Ti^{3+}/[Ti^{4+} + Ti^{3+}]$ and $\beta = Sr_B/[Sr_A + Sr_B]$ is reported in Figs. 5(a) and 5(b), respectively.

Although H2 and H3 show similar trends during both etching and relaxation times, several differences can be noticed. As displayed in Fig. 5(a), at $t = 0$, α is found slightly larger for H3 ($\alpha \approx 3.6\%$) than for H2 ($\alpha < 2\%$), which is compatible with the initially insulating (conductive) character of the interface H2 (H3). In both cases, α increases to reach a similar value (∼8.2%) after 580 s of etching. Then, a slight decrease of α is observed during the 800-min waiting time in the XPS chamber. Finally, both interfaces reach a steady state in which the ratio of Ti atoms in lowered oxidation states is $\alpha \approx 4.2\%$. As shown in Fig. 5(b), a similar evolution occurs for strontium. The fraction $\beta = Sr_B/[Sr_A + Sr_B]$ grows continuously to reach ∼11−13% at the end of the etching. For both samples, β becomes finally equal to 7–8% in the steady state after relaxation processes.

The time evolution of α and β after the end of the cluster ion irradiation is a clear indication of the existence of dynamical processes on Ti and Sr atoms (occurring over several hours) that compete with the effect of the ion exposure. Such relaxation effects have been already reported on titanium after Ar^+ monoatomic ion irradiation of STO substrates and were mainly attributed to the diffusion of ion-induced oxygen vacancies created nearby the surface [35,43]. Here, such a relaxation effect is evidenced for the first time on Ti and Sr atoms in LAO/STO. These dynamical processes are also the reason for the less pronounced chemical modifications on Ti and Sr atoms in H2 and H3 in comparison with H1. Indeed, as counting times were increased between each etching step (68 min instead of 12 min for H1), these relaxation phenomena compete with the effects induced by the ion beam irradiation, resulting in lower values for α and β.

Figure 5(c) shows that a clear modification of the cationic stoichiometry of the LAO film occurs during the cluster ion sputtering. At $t = 0$, the La/Al ratio is 0.9 for both samples, and it grows continuously up to 1.12–1.13. In other words, the LAO layer, which was initially deficient in La (certainly due to the PLD growth conditions: laser energy density, oxygen pressure, deposition temperature), shows La-rich compositions after the ion irradiation. This suggests selective sputtering and Al depletion within the LAO film, likely due to the significant mass mismatch between La and Al ($m_{La}/m_{Al} \approx 5$). No relaxation process is observed in the cationic stoichiometry within the 800 min following the cluster ion beam irradiation. Moreover, for both samples, AFM images of the irradiated area demonstrate that the surface topography is strongly modified [see Figs. SI-5(b) and SI-6(b) of the Supplemental Material [31]]. In particular, the well-defined terraces have disappeared, and the roughness of the sputtered surfaces appears noticeably larger than in as-grown samples.

2. Evolution of the electrical properties

After the cluster ion sputtering and the relaxation processes, we have investigated the evolution of the electrical properties of both interfaces. As for H3, we find that the electrical properties are not noticeably modified on both the irradiated (A) and the witness (B) area. Indeed, no significant change is evidenced in the sheet resistance [Fig. 4(b) and Fig. SI-10 of the Supplemental Material [31]] and the carrier density [Fig. 4(c)]. Conversely, the electrical properties of H2 are significantly modified since the sheet resistance on the area (A) is reduced by two orders of magnitude at room temperature [see Fig. 4(b) and Fig. SI-10 of the Supplemental Material [31] for the temperature dependence of R_S). As a result, the irradiated area becomes almost as conductive as the nonannealed sample H3. As shown in Fig. 4(c), the carrier density of H2 is increased by two orders of magnitude on the irradiated area (A). These electrical measurements are consistent with our XPS data and an occupation of $3d$ levels on Ti atoms (Ti^{3+}), which is responsible for electrical conduction. Indeed, while the ratio α is not appreciably modified after ion exposure and relaxation for H3 (from 3.6% at $t = 0$ to 4.2%), it significantly increases for H2 (<2% at $t = 0$ to 4.2%). An interesting finding is that the electrical resistance of H2 is also decreased on the witness area (B), but to a lesser extent (less than one order of magnitude at 300 K), while the carrier density is increased by one order of magnitude. These observations demonstrate that the large amount of oxygen vacancies, created by the cluster ion beam irradiation on the area (A), diffuse throughout the STO substrate since effects of the ion exposure are detected as far as area (B). Interestingly, in any case, the bare STO area (C) remains perfectly insulating, indicating that oxygen vacancies are undoubtedly stabilized and confined in the vicinity of the interface with LAO.

B. After post-annealing

To confirm the primary role played by oxygen vacancies and to verify whether the electrical properties of the interfaces can be reversibly restored, the two samples H2 and H3 were then annealed (for 1 h at 530 °C in an oxygen pressure of 0.2 mbar) in the same chamber used for the PLD. We observe that the witness area (B) of both samples retrieves the initial electrical properties of annealed interfaces: The electrical resistance [Fig. 4(b) and Fig. SI-10 of the Supplemental Material [31]] and the carrier density [Fig. 4(c)] measured on the area (B) are similar to the initial values obtained for the annealed heterostructure H2 before any irradiation. On the other hand, the irradiated areas (A) are found more insulating than at $t = 0$. For both samples, the sheet resistance is $\sim 6\,M\Omega/\square$ at 300 K, and its temperature dependence is characteristic of a strong localization regime (see Fig. SI-10 of the Supplemental Material [31]). No data for the carrier density are provided on the irradiated areas (A) after annealing, as the sheet resistance was too high to obtain reliable results.

Annealing has the effect of removing the oxygen vacancies present in the heterostructure. This has been confirmed by XPS measurements: After annealing, the Ti^{3+} component of the Ti $2p_{3/2}$ peak is almost completely removed, and the ratio α is found <2% (see Figs. SI-8 and SI-9 of the Supplemental Material [31]). Conversely, XPS spectra reveal that strontium is still strongly modified on the ion-irradiated areas (A) of both samples. The ratio β is equal to 10.6% and 13.2% for H2 and H3, respectively, indicating that Sr atoms are still present at the LAO surface. In addition, AFM images of the irradiated area (A) [see Fig. SI-6(c) of the Supplemental Material [31]] show that annealing has no visible effect on the surface topography, which remains strongly modified. Likewise, the cationic stoichiometry of the LAO film is not changed by the annealing, and the irradiated LAO film is still La rich.

To characterize the local nanostructure of the samples after the cluster ion beam exposure and the following annealing, TEM measurements were performed on the irradiated area (A) of H2. The TEM allowed the verification of the crystallinity and the thickness of the irradiated LAO layer and brought some indications on its compositional evolution through EDS line profile analyses. The observed contrast in high-resolution TEM (HRTEM) images, with the change in bright dot periodicity from 0.28 nm to 0.38 nm, allows the discrimination of the STO substrate from the LAO layer. As well, LAO can be isolated from the so-called Pt-DB layer (deposited for the lamella preparation), which comprises Pt nano-crystals embedded in an amorphous C-based matrix. The TEM images show that the irradiated LAO film appears only slightly altered on some areas [Fig. 6(a)], where the LAO thickness (4.7 nm) is not significantly modified, while it is truly and quite irregularly etched on some other areas where the minimum thickness was found at 2.7 nm [Fig. 6(b)]. Such results are consistent with the mean thickness of 3.5 nm estimated from XPS data, and it confirms the topography of the upper LAO surface measured by AFM. Importantly, it appears that the rough LAO surface topography revealed by the AFM images is not related to an amorphization phenomenon but is rather due to an irregular physical etching of the LAO film by the Ar clusters. Moreover, the observation of visible contrasts on the TEM images at the LAO/STO interface suggests also that the STO framework might have been perturbed to some extent by the ion exposure.

The STEM was also performed. High angle annular dark field imaging, which is a Z-sensitive contrast technique, confirmed the observations of HRTEM images, that is, the LAO layer remains crystalline and exhibits sizeable variations in

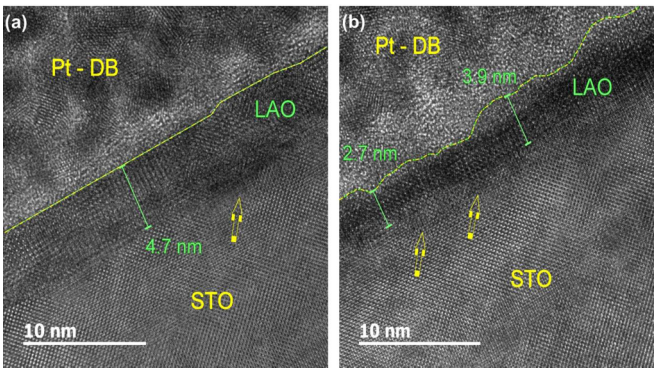

FIG. 6. High-resolution TEM images of post-annealed sample H2 showing the stacking of crystallized LAO layer upon STO substrate. The LAO layer remains mostly crystalline and exhibits visible variations in thickness from (a) 4.7 nm to (b) 2.7 nm. To ease LAO layer visualization, its surface is materialized with a dotted line. Arrows point out the existence of perturbed areas at the LAO/STO interface.

thickness (see Fig. SI-11 in the Supplemental Material [31]). The EDS line profile analyses were also performed across the layer stacking STO/LAO/Pt-DB (see Fig. SI-12 in the Supplemental Material [31]). Two remarks can be drawn from these analyses: Both LAO/Pt-DB and LAO/STO interfaces appear rather rough. In addition, the evolution of the net intensity of the Sr L peak appears to be compatible with a migration of Sr atoms towards the LAO surface.

V. GENERAL DISCUSSION AND CONCLUSIONS

In this second part, we have studied the evolution of the electrical properties of LAO/STO interfaces under the effect of a short-time argon cluster ion beam irradiation. This investigation was carried out combining XPS and electrical transport measurements, which provide complementary information on both the chemistry and the physics of the heterointerface and possible correlations between them. Contrary to what was generally observed by using high-energy ion beam irradiation techniques, we find that the cluster ion beam exposure can induce an increase of the electrical conductivity at the LAO/STO interface. This is undoubtedly correlated to the unique features of this low-energy sputtering technique in perovskite oxide materials (low energy per incoming Ar atom, low sputter rate, and negligible argon implantation) [34,35]. Interestingly, even if the buried STO is most likely *not directly* affected by the Ar clusters, XPS data revealed that the main modifications are observed on Sr and Ti atoms near the interface. In particular, a lowering of the mean oxidation state of titanium and the apparition of a new chemical environment for strontium, attributed to a migration of Sr atoms toward the LAO surface, were clearly observed.

One of the first effects of the cluster ion exposure is to induce chemical modifications in the LAO film. Indeed, a clear increase of the La/Al ratio is measured on the irradiated areas. This reveals a selective sputtering of light Al atoms likely due to the large mass mismatch between La and Al ($m_{La}/m_{Al} \approx 5$). We can mention that such a selective sputtering by the cluster ion source was not observed on STO substrates [35] because the mismatch between Sr and Ti is significantly smaller ($m_{Sr}/m_{Al} \approx 1.8$). Furthermore, it is worth mentioning that the topography of the upper LAO surface is strongly modified by the cluster ion irradiation, as revealed by AFM and TEM images.

In STO, the appearance of low oxidation states of Ti atoms is related to the formation of oxygen vacancies near the interface into the buried STO substrate. These oxygen vacancies are undoubtedly formed in the LAO layer before diffusing into STO. This assumption is supported by several arguments. First, in similar irradiation conditions, we observed a significant larger fraction of Ti^{3+} and Ti^{2+} ions in the case of the LAO/STO interface than in a pure STO substrate, indicating that LAO plays a key role in the formation of oxygen vacancies. Second, the relaxation process (occurring over several hours) evidenced on the XPS Ti $2p_{3/2}$ core-line is consistent with a diffusion phenomenon of oxygen vacancies into STO and in the entire heterostructure. These results indicate that the LAO film acts as a magnifier in injecting oxygen vacancies into STO. Such a behavior has been confirmed by *ab-initio* calculations [51], which show that the formation energies of oxygen vacancies in LAO are lower than in STO.

Buried strontium atoms are also remarkably affected by the cluster ion irradiation of the LAO surface. The formation of the high-binding energy component revealed by XPS is associated to the migration of Sr atoms toward the outermost surface (through the LAO film) due to the destabilization of the thermodynamic equilibrium of the heterostructure by the ion etching. Indeed, the LEIS measurements revealed a noticeable enrichment of the upper surface with Sr atoms on the irradiated areas. It is worth mentioning that such a migration of Sr atoms toward the surface is a well-known property already observed in STO when some energy is provided to the system, either by high-temperature annealing [47] or by ion sputtering [34,40,41]. The mechanism at the origin of Sr migration in LAO/STO is not perfectly understood, and further investigations should be done to explain this effect. We can speculate that the thermodynamic disturbance of the interface by the ion irradiation may favor the migration of Sr into the LAO film in two different ways: La-Sr intermixing, which is an expected phenomenon [52], or filling of ion-induced aluminum vacancies in LAO by Sr atoms. Otherwise, there is no apparent correlation between the modification rates of Ti and Sr. Indeed, as displayed in Figs. 5(a) and 5(b), the modification rate of Ti is much faster than that of Sr, in particular in the early stages of the etching, suggesting that the migration of Sr atoms is not directly related to the creation of oxygen vacancies.

It should be stressed that the observed modifications in STO are undoubtedly attributed to cluster-ion-induced processes, rather than static effects being already present in the LAO film and revealed by XPS and LEIS probes only due to the physical etching of the layer. On one hand, this is proved by the fact that these modifications are *always* the subject of dynamical relaxation processes clearly evidenced on both XPS Ti and Sr peaks (*vide infra*). Second, complementary XPS measurements, performed on thinner heterointerfaces (3.5 nm, i.e., a similar thickness to the one estimated for H2 and H3 after the ion exposure), demonstrated the absence of these features on thin as-grown samples.

All these chemical changes detected by XPS are the cause of deep modifications in the electronic properties of the interfaces. Despite the change of the chemical environment of Sr atoms and the La/Al ratio, an increase of the electrical conductivity is observed at the LAO/STO interface after the ion beam irradiation. This effect is more especially pronounced for the initially insulating interface H2 in which the sheet resistance is reduced by two orders of magnitude at room temperature. In the case of the nonannealed interface H3, the effect of the ion irradiation on the electrical properties is less pronounced, certainly because the interface is already saturated with oxygen vacancies.

Earlier studies have reported that only Al-rich LAO films result in conductive heterointerfaces [53,54]. Such outcomes are not verified in our case since the interfacial conductivity seems to be primarily driven by the formation of ion-induced oxygen vacancies. This point of view is supported by the fact that the removal of oxygen vacancies by post-annealing leads to a more insulating interface on the ion-irradiated area. This effect cannot be imputed to the physical etching of the LAO film below the 4-u.c. critical threshold for electrical conductivity because the mean thickness (estimated from XPS data) is ∼3.5 nm (∼9 u.c.) after the cluster ion beam irradiation. This was further confirmed by the HRTEM images that show that in spite of a quite irregular physical etching, the crystallinity of the LAO film is preserved for a minimal thickness of 2.7 nm (∼7 u.c.). Instead, some other effects could explain this observation since the irradiated areas remain chemically modified after annealing. In this way, the modified cationic stoichiometry ($La/Al > 1$) [53] or the migration of strontium atoms toward the surface could be possible reasons for a larger resistivity after annealing. Nevertheless, we cannot definitely rule out the possible formation of local defects/strains in the LAO layer or in the buried STO substrate due to the ion exposure.

Another striking result of our paper is the existence of dynamical processes, which compete with the effect of the cluster ion beam irradiation. These relaxation phenomena have been evidenced by XPS on both Ti and Sr peaks. For titanium, such a relaxation process is attributed to the diffusion of the ion-beam-induced oxygen vacancies near the interface in the entire heterostructure. This effect has been confirmed by electrical transport measurements since an increase of the conductivity was also observed on the witness area (B) after the ion irradiation. The origin of this relaxation process on Sr atoms is more debatable, but it might be related to the diffusion process of Sr atoms in the LAO film. In any case, the fact that these dynamical processes occur over several hours clearly indicates that atomic relaxation phenomena must be considered instead of purely electronic relaxation processes.

Our findings can be put in perspective with the results obtained by Aurino *et al.* [27,28] using 150–350 eV argon monoatomic ions. The authors observed different regimes according to the energy of incoming ions. While a decrease of the electrical resistance was evidenced for relatively high energetic ions (350 eV) due to the formation of oxygen vacancies, a spectacular increase of the resistivity was observed at low energy (150 eV) in the first stages of the ion exposure [28]. In such a low-energy regime, it appears that the monoatomic irradiation first induces ion-beam defects in the LAO layer through argon implantation [27], which eliminate the electrical conductivity, and only after some etching generates defects (oxygen vacancies) into the interface, as demonstrated by the following decrease of the resistivity for longer etching times. The sputtering process of clusters over a long period of time appears to be more complex than that of monoatomic ions in the sense that highly nonlinear collision cascades and then nonlinear energy deposition are expected on the sputtered surface [55]. Even though no detectable Ar implantation occurs and the average energy per incoming argon atom is considerably low, the cluster ion sputtering seems to roughen the irradiated upper surface, as revealed by the irregular surface topography. As a result, immediate effects (change of stoichiometry, oxygen vacancies, and Sr migration) are detected near the interface and in deep layers of the heterostructure to compensate the ion-induced imbalance, resulting in an increase of the electrical conductivity as soon as the first stages of the ion exposure. Interestingly, in opposition to our observations, no dynamical effects, in particular on the Sr atoms, were reported using the monoatomic ion irradiation.

In conclusion, this paper gives new experimental insights into the physics of the LAO/STO interface and, in particular, into the influence of local ion-induced perturbations on the electronic properties of the q-2-DEG. Importantly, the primary role played by oxygen vacancies created within the LAO layer has been emphasized. Further studies need to be performed to determine the influence of the characteristics of the cluster ion irradiation (cluster energy and size) as well as the initial properties of LAO/STO heterostructures (such as stoichiometry or thickness) on the different phenomena (chemical, compositional, and electronic modifications) induced by the Ar cluster ion beam exposure.

ACKNOWLEDGMENTS

This work was performed with the financial support of the programs OxyCAR II, Ile-de-France region DIM OxyMore for XPS measurements; NOVATECH C'Nano Ile-de-France (Project No. IF-08-1453/R) for electrical measurements; and EQUIPEX GENESIS, Agence Nationale de la Recherche (ANR-11-EQPX-0020) for TEM lamella preparation. K.R. is grateful to the Labex CHARMMMAT for the postdoctoral grant.

The authors declare no competing financial interest.

[1] A. Ohtomo and H. Y. Hwang, Nature **427**, 423 (2004).

[2] S. Thiel, G. Hammerl, A. Schmehl, C. W. Schneider, and J. Mannhart, Science **313**, 1942 (2006).

[3] A. Brinkman, M. Huijben, M. van Zalk, J. Huijben, U. Zeitler, J. C. Maan, W. G. van der Wiel, G. Rijnders, D. H. A. Blank, and H. Hilgenkamp, Nat. Mater. **6**, 493 (2007).

[4] Ariando, X. Wang, G. Baskaran, Z. Q. Liu, J. Huijben, J. B. Yi, A. Annadi, A. R. Barman, A. Rusydi, S. Dhar, Y. P. Feng, J. Ding, H. Hilgenkamp, and T. Venkatesan, Nat. Commun. **2**, 188 (2011).

[5] J. A. Bert, B. Kalisky, C. Bell, M. Kim, Y. Hikita, H. Y. Hwang, and K. A. Moler, Nat. Phys. **7**, 767 (2011).

[6] T. Taniuchi, Y. Motoyui, K. Morozumi, T. C. Rödel, F. Fortuna, A. F. Santander-Syro, and S. Shin, Nat. Commun. **7**, 11781 (2016).

[7] N. Reyren, S. Thiel, A. D. Caviglia, L. F. Kourkoutis, G. Hammerl, C. Richter, C. W. Schneider, T. Kopp, A.-S. Ruetschi, D. Jaccard, M. Gabay, D. A. Muller, J.-M. Triscone, and J. Mannhart, Science **317**, 1196 (2007).

[8] A. D. Caviglia, M. Gabay, S. Gariglio, N. Reyren, C. Cancellieri, and J.-M. Triscone, Phys. Rev. Lett. **104**, 126803 (2010).

[9] M. Ben Shalom, M. Sachs, D. Rakhmilevitch, A. Palevski, and Y. Dagan, Phys. Rev. Lett. **104**, 126802 (2010).

[10] N. Nakagawa, H. Y. Hwang, and D. A. Muller, Nat. Mater. **5**, 204 (2006).

[11] W. Siemons, G. Koster, H. Yamamoto, W. A. Harrison, G. Lucovsky, T. H. Geballe, D. H. A. Blank, and M. R. Beasley, Phys. Rev. Lett. **98**, 196802 (2007).

[12] A. Kalabukhov, R. Gunnarsson, J. Börjesson, E. Olsson, T. Claeson, and D. Winkler, Phys. Rev. B **75**, 121404 (2007).

[13] G. Herranz, M. Basletic, M. Bibes, C. Carrétéro, E. Tafra, E. Jacquet, K. Bouzehouane, C. Deranlot, A. Hamzic, J.-M. Broto, A. Barthélémy, and A. Fert, Phys. Rev. Lett. **98**, 216803 (2007).

[14] P. R. Willmott, S. A. Pauli, R. Herger, C. M. Schlepütz, D. Martoccia, B. D. Patterson, B. Delley, R. Clarke, D. Kumah, C. Cionca, and Y. Yacoby, Phys. Rev. Lett. **99**, 155502 (2007).

[15] A. S. Kalabukhov, Y. A. Boikov, I. T. Serenkov, V. I. Sakharov, V. N. Popok, R. Gunnarsson, J. Börjesson, N. Ljustina, E. Olsson, D. Winkler, and T. Claeson, Phys. Rev. Lett. **103**, 146101 (2009).

[16] L. Yu and A. Zunger, Nat. Commun. **5**, 5118 (2014).

[17] A. D. Caviglia, S. Gariglio, N. Reyren, D. Jaccard, T. Schneider, M. Gabay, S. Thiel, G. Hammerl, J. Mannhart, and J.-M. Triscone, Nature **456**, 624 (2008).

[18] D. F. Bogorin, P. Irvin, C. Cen, and J. Levy, in *Multifunct. Oxide Heterostruct.*, edited by E. Y. Tsymbal, E. R. A. Dagotto, C.-B. Eom, and R. Ramesh (Oxford University Press, 2012), pp. 364–388.

[19] C. Cen, S. Thiel, G. Hammerl, C. W. Schneider, K. E. Andersen, C. S. Hellberg, J. Mannhart, and J. Levy, Nat. Mater. **7**, 298 (2008).

[20] Y. Xie, C. Bell, T. Yajima, Y. Hikita, and H. Y. Hwang, Nano Lett. **10**, 2588 (2010).

[21] W. Dai, S. Adhikari, A. C. Garcia-Castro, A. H. Romero, H. Lee, J.-W. Lee, S. Ryu, C.-B. Eom, and C. Cen, Nano Lett. **16**, 2739 (2016).

[22] Y. Xie, Y. Hikita, C. Bell, and H. Y. Hwang, Nat. Commun. **2**, 494 (2011).

[23] K. A. Brown, S. He, D. J. Eichelsdoerfer, M. Huang, I. Levy, H. Lee, S. Ryu, P. Irvin, J. Mendez-Arroyo, C.-B. Eom, C. A. Mirkin, and J. Levy, Nat. Commun. **7**, 10681 (2016).

[24] X. Xiang, L. Qiao, H. Y. Xiao, F. Gao, X. T. Zu, S. Li, and W. L. Zhou, Sci. Rep. **4**, 5477 (2014).

[25] A. V. Krasheninnikov and K. Nordlund, J. Appl. Phys. **107**, 071301 (2010).

[26] T. Wolf, N. Bergeal, J. Lesueur, C. J. Fourie, G. Faini, C. Ulysse, and P. Febvre, IEEE Trans. Appl. Supercond. **23**, 1101205 (2013).

[27] P. P. Aurino, A. Kalabukhov, N. Tuzla, E. Olsson, A. Klein, P. Erhart, Y. A. Boikov, I. T. Serenkov, V. I. Sakharov, T. Claeson, and D. Winkler, Phys. Rev. B **92**, 155130 (2015).

[28] P. P. Aurino, A. Kalabukhov, N. Tuzla, E. Olsson, T. Claeson, and D. Winkler, Appl. Phys. Lett. **102**, 201610 (2013).

[29] S. Mathew, A. Annadi, T. K. Chan, T. C. Asmara, D. Zhan, X. R. Wang, S. Azimi, Z. Shen, A. Rusydi, Ariando, M. B. H. Breese, and T. Venkatesan, ACS Nano **7**, 10572 (2013).

[30] S. Hurand, A. Jouan, C. Feuillet-Palma, G. Singh, E. Lesne, N. Reyren, A. Barthélémy, M. Bibes, J. E. Villegas, C. Ulysse, M. Pannetier-Lecoeur, M. Malnou, J. Lesueur, and N. Bergeal, Appl. Phys. Lett. **108**, 052602 (2016).

[31] See Supplemental Material at http://link.aps.org/supplemental/10.1103/PhysRevB.97.035146 for summary table of experimental ion beam irradiations performed on LAO/STO heterostructures. Additional results on the depth profiling analysis of the LAO/STO heterostructure H1: estimation of the LAO thickness from XPS measurements, XPS La 4*d*, Al 2*p* and valence band spectra, and comparison with a cluster ion beam irradiation performed on a bare STO substrate. Additional results on the short-time argon cluster ion exposures performed on the LAO/STO heterostructures H2 and H3: AFM images of the irradiated areas, XPS Ar 2*p*, Ti $2p_{3/2}$ and Sr 3*d* spectra, thermal dependence of the sheet resistance on both areas (A) and (B), and electron microscopy study of the heterostructure H2.

[32] J. L. S. Lee, S. Ninomiya, J. Matsuo, I. S. Gilmore, M. P. Seah, and A. G. Shard, Anal. Chem. **82**, 98 (2010).

[33] D. Rading, R. Moellers, H.-G. Cramer, and E. Niehuis, Surf. Interface Anal. **45**, 171 (2013).

[34] D. Aureau, K. Ridier, B. Bérini, Y. Dumont, N. Keller, J. Vigneron, M. Bouttemy, A. Etcheberry, and A. Fouchet, Thin Solid Films **601**, 89 (2016).

[35] K. Ridier, D. Aureau, B. Bérini, Y. Dumont, N. Keller, J. Vigneron, A. Etcheberry, and A. Fouchet, J. Phys. Chem. C **120**, 21358 (2016).

[36] M. P. Seah, Surf. Interface Anal. **44**, 1353 (2012).

[37] V. E. Henrich, G. Dresselhaus, and H. J. Zeiger, Phys. Rev. B **17**, 4908 (1978).

[38] G. Drera, F. Banfi, F. F. Canova, P. Borghetti, L. Sangaletti, F. Bondino, E. Magnano, J. Huijben, M. Huijben, G. Rijnders, D. H. A. Blank, H. Hilgenkamp, and A. Brinkman, Appl. Phys. Lett. **98**, 052907 (2011).

[39] A. Koitzsch, J. Ocker, M. Knupfer, M. C. Dekker, K. Dörr, B. Büchner, and P. Hoffmann, Phys. Rev. B **84**, 245121 (2011).

[40] Y. Adachi, S. Kohiki, K. Wagatsuma, and M. Oku, Appl. Surf. Sci. **143**, 272 (1999).

[41] B. Psiuk, J. Szade, M. Pilch, and K. Szot, Vacuum **83**, S69 (2009).

[42] D. Kan, T. Terashima, R. Kanda, A. Masuno, K. Tanaka, S. Chu, H. Kan, A. Ishizumi, Y. Kanemitsu, Y. Shimakawa, and M. Takano, Nat. Mater. **4**, 816 (2005).

[43] M. Schultz and L. Klein, Appl. Phys. Lett. **91**, 151104 (2007).

[44] G. Herranz, O. Copie, A. Gentils, E. Tafra, M. Basletić, F. Fortuna, K. Bouzehouane, S. Fusil, é. Jacquet, C. Carrétéro, M. Bibes, A. Hamzić, and A. Barthélémy, J. Appl. Phys. **107**, 103704 (2010).

[45] A. F. Santander-Syro, O. Copie, T. Kondo, F. Fortuna, S. Pailhès, R. Weht, X. G. Qiu, F. Bertran, A. Nicolaou, A. Taleb-Ibrahimi, P. Le Fèvre, G. Herranz, M. Bibes, N. Reyren, Y. Apertet, P. Lecoeur, A. Barthélémy, and M. J. Rozenberg, Nature **469**, 189 (2011).

[46] P. A. W. Van der Heide, Q. D. Jiang, Y. S. Kim, and J. W. Rabalais, Surf. Sci. **473**, 59 (2001).

[47] K. Szot, W. Speier, U. Breuer, R. Meyer, J. Szade, and R. Waser, Surf. Sci. **460**, 112 (2000).

[48] H. Wei, L. Beuermann, J. Helmbold, G. Borchardt, V. Kempter, G. Lilienkamp, and W. Maus-Friedrichs, J. Eur. Ceram. Soc. **21**, 1677 (2001).

[49] S. Gerhold, Z. Wang, M. Schmid, and U. Diebold, Surf. Sci. **621**, L1 (2014).

[50] M. Huijben, A. Brinkman, G. Koster, G. Rijnders, H. Hilgenkamp, and D. H. A. Blank, Adv. Mater. **21**, 1665 (2009).

[51] Y. Li, S. N. Phattalung, S. Limpijumnong, J. Kim, and J. Yu, Phys. Rev. B **84**, 245307 (2011).

[52] A. Kalabukhov, Y. A. Boikov, I. T. Serenkov, V. I. Sakharov, J. Börjesson, N. Ljustina, E. Olsson, D. Winkler, and T. Claeson, EPL Europhys. Lett. **93**, 37001 (2011).

[53] M. P. Warusawithana, C. Richter, J. A. Mundy, P. Roy, J. Ludwig, S. Paetel, T. Heeg, A. A. Pawlicki, L. F. Kourkoutis, M. Zheng, M. Lee, B. Mulcahy, W. Zander, Y. Zhu, J. Schubert, J. N. Eckstein, D. A. Muller, C. S. Hellberg, J. Mannhart, and D. G. Schlom, Nat. Commun. **4**, 2351 (2013).

[54] E. Breckenfeld, N. Bronn, J. Karthik, A. R. Damodaran, S. Lee, N. Mason, and L. W. Martin, Phys. Rev. Lett. **110**, 196804 (2013).

[55] I. Yamada, J. Matsuo, N. Toyoda, and A. Kirkpatrick, Mater. Sci. Eng. R Rep. **34**, 231 (2001).